Strongly Interacting Organic Conjugated Dendrimers with Enhanced Two-Photon Absorption

ARTICLE *in* THE JOURNAL OF PHYSICAL CHEMISTRY C · NOVEMBER 2006

Impact Factor: 4.77 · DOI: 10.1021/jp0640068

Strongly Interacting Organic Conjugated Dendrimers with Enhanced Two-Photon Absorption

Oleg Varnavski,[†] Xingzhong Yan,[†] Olivier Mongin,[‡] Mireille Blanchard-Desce,*[,‡] and Theodore Goodson, III*[,†]

Department of Chemistry, NSF Center for Ultra-fast Optical Science (FOCUS), University of Michigan, Ann Arbor, Michigan 48109, and Synthèse et ElectroSynthèse Organiques (CNRS, UMR 6510), Université de Rennes 1, Institut de Chimie, Campus Scientifique de Beaulieu, Bât 10A, F-35042 Rennes Cedex, France

Received: June 26, 2006; In Final Form: October 10, 2006

We report a strongly interacting new dendrimer system with an extended spectroscopic unit (coherent domain) beyond the trimer configuration. This report focuses on the mechanism of enhancement of the two-photon absorption (TPA) response of this material as a function of the dendrimer generation number. This enhancement is strongly correlated to the size and geometry of the spectroscopic unit in a strongly interacting macromolecular system. These systems are investigated by a wide variety of time-resolved spectroscopy methods including time-resolved fluorescence, transient absorption, three-pulse photon echo peak shift measurements as well as TPA cross section measurements. The extensive combination of modern spectroscopic methods strongly indicates that the spectroscopic unit (domain) in high generations covers the G1 (nine linear building blocks) and exceeds the trimer size.

1. Introduction

Recent interest in the use of organic branched (dendritic) structures for nonlinear optical (NLO) applications have motivated the synthesis and characterization of many new and intriguing structures.[1,2] A great deal of this enthusiasm stems from the possibility that nonlinear properties (in particular two-photon absorption (TPA) effect) in the branching architecture may be enhanced as compared to its linear counterparts.[3−6] From the earliest reports of enhancement in branching structures the challenge of reaching very large cross sections has been met with a close connection of synthesis and photophysical structure−property characterization. The dendrimer architecture has also been found very promising for light-harvesting antenna applications in synthetic solar cells as well as for organic light-emitting diodes.[7−12] A fundamental advantage of dendrimers over the conventional linear polymers in optical applications is mostly associated with the possibility of concentrating a large number of chromophores in an ordered confined geometry which grows exponentially with the generation number.[13,14] This advantage can be realized either in conjugated dendrimers where intrinsic conjugated linear building blocks are connected through the branching centers[15−18] or in chromophore-labeled systems where the optically inactive dendrimer is mostly used as a framing scaffold for the chromophores.[19−21] In conjugated dendrimers, a higher density of effective chromophores as well as strong interchromophore coupling can be achieved, which is important for many nonlinear optical and light-harvesting applications.[1−6,22,23] As the branching centers in such dendrimers can potentially disrupt the conjugation, the conjugated dendrimer can be often viewed as an ensemble of interacting conjugated blocks (chromophores).[24−26] The size of the chromophores and the coupling strength between them are the key parameters for light-harvesting applications as well as for nonlinear optical enhancement over the additive behavior.[1−6,27,28] The phenylacetylene dendrimer family is the most extensively investigated conjugated dendrimer system both theoretically and experimentally.[7,15,24−26,29−31] It was shown that in the ground-state configuration the chromophore unit can be associated with a single, linear building block and the effective interaction between these chromophores is in a weak coupling limit, thus suggesting incoherent hopping of excitation at room temperature.[24,25] In order to get ultrafast nonlinear responses (similar to two-photon absorption cross section) enhanced beyond the additive limit in a large multichromophore system, strong interchromophore coupling is necessary in the ground-state configuration.[1−6] Strong interchromophore (interbranch) coupling leading to delocalized excitations can also be beneficial for light-harvesting applications. However, only a limited number of conjugated dendrimers containing large numbers of strongly coupled conjugated blocks have been experimentally investigated,[28,32] although the strongly interacting three-branched system (trimer) has recently received considerable attention, and the possibility of the enhancement of the second- and third-order nonlinearities beyond the additive behavior relation has been established in such trimer systems.[1−6,33] In our previous publication we have shown that the delocalization length of the electronic wave function (coherent domain) size in a real dendrimer can rise with the increase of the generation number G up to $G = 3$.[34] In the case of the TPA in dendrimers larger than trimer, the enhancement effect has been first reported in four-branched stilbenyl dendrimers which can be also interpreted in terms of coherent domains extending beyond the trimer configuration.[28] However, its connection to the structure of excitations in dendrimers (interbranch coupling, excitation dynamics) has not been investigated.

Because of the fact that in large conjugated dendrimers with strong interbranch coupling the delocalization of the electronic wavefunction can exceed the size of one linear segment, it is

* Corresponding authors. E-mail: tgoodson@umich.edu; mireille.blanchard-desce@univ-rennesl.fr.
[†] Department of Chemistry, University of Michigan.
[‡] Université de Rennes 1, Institut de Chimie.

10.1021/jp0640068 CCC: $37.00
Published on Web 11/23/2006

SCHEME 1: Molecular Structures of Dendrimers G0, G1, G2, and Model Linear Block LB

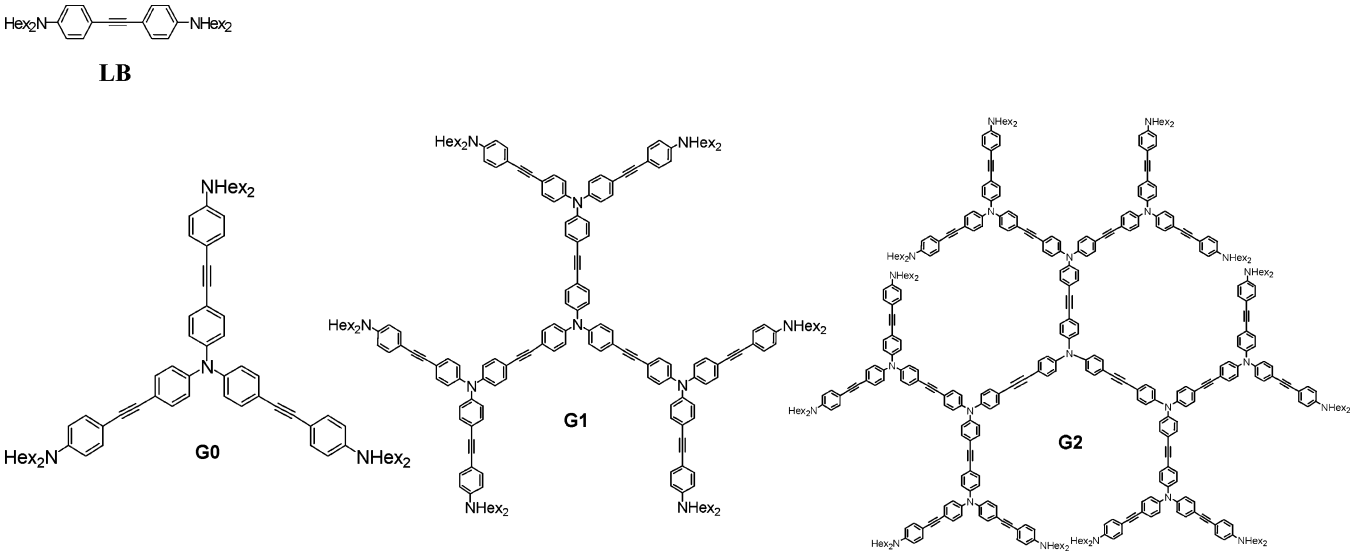

useful to introduce a concept of spectroscopic unit similar to that used for linear polymers.[35−38] It describes the domain over which the excitation is delocalized in the dendrimer. If the domain size is smaller than the size of the dendrimer molecule, this macromolecule can be viewed as an ensemble of the spectroscopic units, and the optical excitation can migrate between the spectroscopic units via an incoherent hopping mechanism.[35−38] This concept is closely related to the diagonal size L_d for electronic modes[25,39] which reflects the size over which the center of mass of the electron−hole pair is distributed.[39] As the electron−hole separation distribution length L_c[39] (charge transfer through the branching center) is not exactly specified, this concept is not limited by a strict Frenkel exciton approximation. The size and geometry of the spectroscopic unit in large dendrimers plays a crucial role in nonlinear response enhancement as well as in light-harvesting applications of large dendrimers.

In this paper we report the synthesis and detailed optical properties of a new, strongly coupled, large conjugated dendrimer (Scheme 1) based on rigid tolane linear building blocks connected through nitrogen branching centers. Nitrogen was shown to be very efficient branching center providing strong interbranch coupling and TPA enhancement.[1−6] New dendrimers demonstrated high quantum yield up to the second generation (21 linear building blocks) with strong coupling leading to the spectroscopic unit beyond the trimer configuration and an enhanced TPA cross section. The focus of this contribution is to probe the spectroscopic unit and structure−function relationship important to the TPA process beyond the situation of the trimer. While time-resolved spectroscopy techniques probe physical events after the excitation has taken place, these methods are very often the only possible means to fully characterize the states which are important to instantaneous TPA and thus derive proper structure−properties relationships. Transient absorption and resonant four-wave mixing experiments can provide information about exact energy-level structure, delocalization length, transition dipoles, and line broadening mechanisms of Frank−Condon states, and these are all critical parameters for TPA enhancement.[4] Fluorescence dynamics can characterize the reorganization (the change in spectroscopic unit) taking place during the relaxation process which is of vital importance for light harvesting or TPA-based sensing applications.[40] Combined with other methods, the ultrafast time-resolved spectroscopy in some cases can also provide indirect information about initial (Frank−Condon) states (e.g., symmetry, extent of delocalization[1,2,41]).

2. Experiment and Numerical Simulation

Synthesis of the Dendrimers. Dendrimers **G0**,[42] **G1**, and **G2** were synthesized by a convergent growth approach[43] based on acetylene linkages.[15] The AB_2 building block **1b** was used to prepare, via iterative Sonogashira couplings and silane deprotections, monodendrons **3b** and **4b**, which were reacted with triiodo core **1a** to afford **G1** and **G2**, respectively (Scheme 2).

Dendrimer G0: mp 93−94 °C. ^{1}H NMR (200.13 MHz, $CDCl_3$) δ 7.38 and 7.03 (AA′XX′, J_{AX} = 8.7, 12H), 7.34 and 6.56 (AA′XX′, J_{AX} = 8.8, 12H), 3.27 (t, J = 7.5, 12H), 1.56 (m, 12H), 1.31 (m, 36H), 0.90 (t, J = 6.4, 18H); ^{13}C NMR (50.32 MHz, $CDCl_3$) δ 147.7, 146.0, 132.7, 132.2, 123.8, 118.7, 111.1, 108.8, 90.5, 86.9, 50.9, 31.7, 27.1, 26.8, 22.6, 14.0; HRMS (LSIMS$^+$, mNBA) calcd for $C_{78}H_{102}N_4$ ($M^{+\bullet}$) m/z 1094.8105, found 1094.8099. Anal. Calcd for $C_{78}H_{102}N_4$ (1095.69): C, 85.50; H, 9.38; N, 5.11. Found: C, 85.27; H, 9.32; N, 5.17.

Dendrimer G1: mp 84−85 °C. ^{1}H NMR (200.13 MHz, $CDCl_3$): δ 7.42 and 7.07 (AA′XX′, J_{AX} = 8.2 Hz, 12H), 7.39 and 7.04 (AA′XX′, J_{AX} = 8.2 Hz, 36H), 7.35 and 6.56 (AA′XX′, J_{AX} = 8.8 Hz, 24H), 3.27 (t, J = 7.4, 24H), 1.58 (m, 24H), 1.31 (m, 72H), 0.90 (t, J = 6.4, 36H); ^{13}C NMR (50.32 MHz, $CDCl_3$) δ 147.8, 146.8, 146.5, 145.9, 132.7, 132.6, 132.5, 132.3, 124.1, 124.0, 123.5, 119.0, 118.1, 117.4, 111.1, 108.8, 90.6, 89.3, 88.9, 86.8, 50.9, 31.7, 27.1, 26.8, 22.6, 14.0; ES$^+$-MS (CH_3OH/CH_2Cl_2: 10/90) m/z 2746.8 ([M + H]$^+$), 1373.9 ([M + 2H]$^{2+}$), 916.4 ([M + 3H]$^{3+}$), 687.7 ([M + 4H]$^{4+}$); HRMS (ES$^+$, CH_3OH/CH_2Cl_2: 10/90) calcd for $C_{198}H_{230}N_{10}$ ([M + 2H]$^{2+}$) m/z 1373.9153, found 1373.9174. Anal. Calcd for $C_{198}H_{228}N_{10}$ (2748.07): C, 86.54; H, 8.36; N, 5.10. Found: C, 86.69; H, 8.41; N, 5.06.

Dendrimer G2: mp 163−164 °C. ^{1}H NMR (300.13 MHz, $CDCl_3$): δ 7.42 and 7.07 (AA′XX′, J_{AX} = 8.7 Hz, 48H), 7.39 and 7.04 (AA′XX′, J_{AX} = 9.2 Hz, 72H), 7.34 and 6.56 (AA′XX′, J_{AX} = 8.6 Hz, 48H), 3.26 (t, J = 7.5, 48H), 1.57 (m, 48H), 1.31 (m, 144H), 0.90 (t, J = 6.5, 72H); ^{13}C NMR (50.32 MHz, $CDCl_3$) δ 147.7, 146.8, 146.5, 146.44, 146.39, 145.8, 132.7, 132.6, 132.5, 132.3, 124.1, 123.9, 123.4, 119.0, 118.1, 118.0, 117.9, 117.3, 111.1, 108.7, 90.6, 89.3, 89.2, 89.1, 88.9, 86.8,

SCHEME 2: Synthesis of Dendrimers[a]

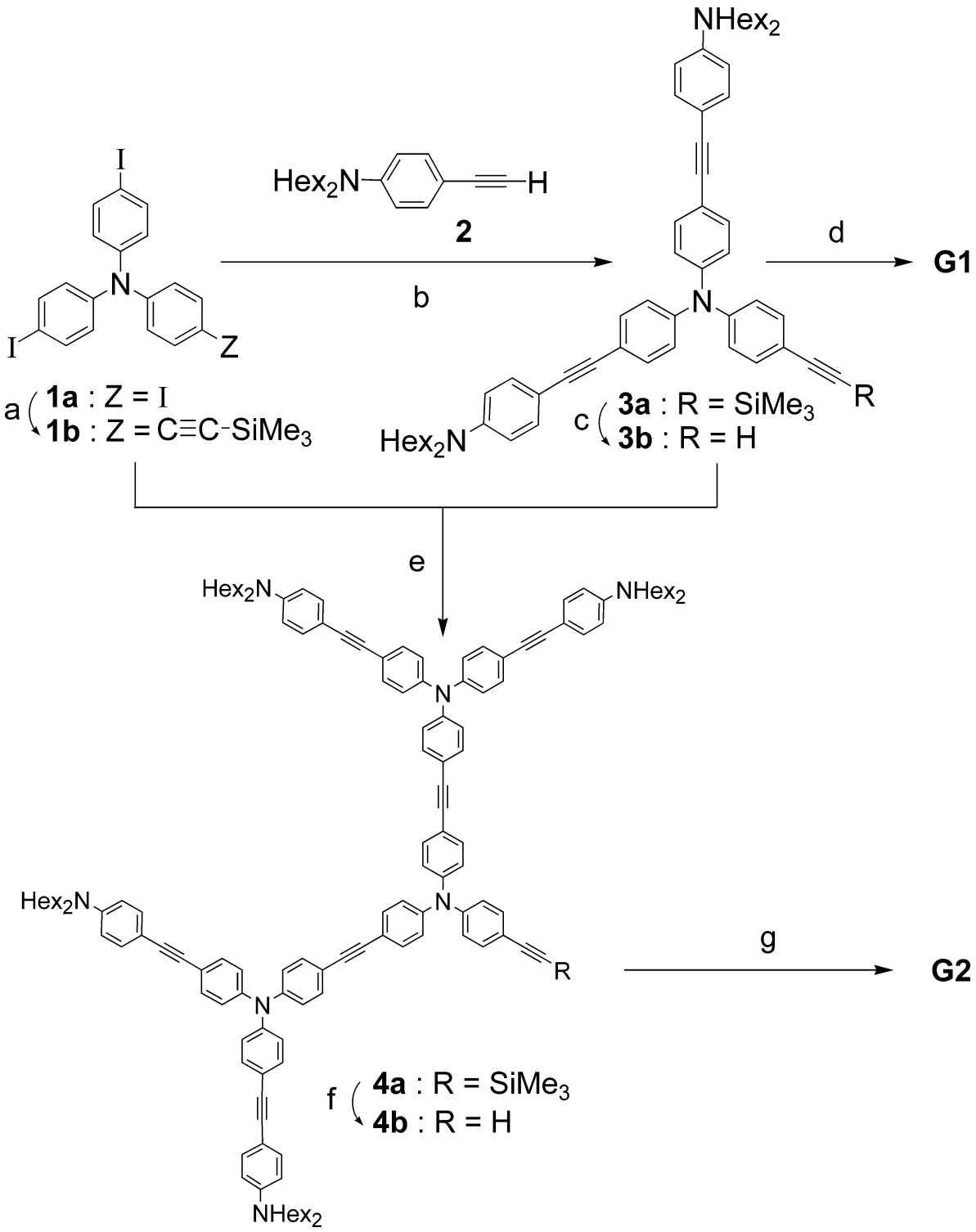

[a] Reagents and conditions: (a) ethynyltrimethylsilane (1 equiv), $Pd(PPh_3)_2Cl_2$, CuI, toluene/Et_3N (37%); (b) **1b** (1 equiv), **2** (3 equiv), $Pd(PPh_3)_2Cl_2$, CuI, toluene/Et_3N (93%); (c) 0.5 N NaOH, THF, 25 °C (93%); (d) **1a** (1 equiv), **3b** (4 equiv), $Pd(PPh_3)_2Cl_2$, CuI, toluene/Et_3N, 40 °C (86%); (e) **1b** (1 equiv), **3b** (3 equiv), conditions as in b (87%); (f) conditions as in c (98%); (g) **1a** (1 equiv), **4b** (4 equiv), conditions as in d (75%).

50.9, 31.6, 27.1, 26.7, 22.6, 14.0; ES^+-MS (CH_3OH/CH_2Cl_2: 10/90) *m/z* 3027.4 ($[M + 2H]^{2+}$), 2018.3 ($[M + 3H]^{3+}$), 1514.0 ($[M + 4H]^{4+}$), 1211.6 ($[M + 5H]^{5+}$); HRMS (ES^+, CH_3OH/CH_2Cl_2: 10/90) calcd for $C_{438}H_{484}N_{22}$ ($[M + 4H]^{4+}$) *m/z* 1512.9637, found 1512.9667. Anal. Calcd for $C_{438}H_{480}N_{22}$ (6052.81): C, 86.92; H, 7.99; N, 5.09. Found: C, 87.13; H, 8.16, N, 5.23.

Steady-State Measurements. UV/vis spectra were recorded on a Jasco V-570 spectrophotometer. Steady-state and time-resolved fluorescence measurements were performed at room temperature in dilute solutions ($\sim 10^{-6}$ M) using an Edinburgh Instruments (FLS 920) spectrometer in photon-counting mode. Emission spectra were obtained, for each compound, at $\lambda_{ex} = \lambda_{max}(abs)$ with $A_{\lambda_{ex}} \leq 0.1$ to minimize internal absorption. Fluorescence quantum yields were measured on degassed samples at room temperature; fluorescein in 0.1 N NaOH was used as a standard (quantum yield $\Phi = 0.90$). The lifetime values were obtained from the reconvolution fit analysis of the

decay profiles with the F900 analysis software, and the fitting results were judged by the reduced χ^2 value.

TPEF measurements were conducted using a mode-locked Ti:sapphire laser operating between 700 and 1000 nm and delivering 80-fs pulses at 80 MHz, following the experimental protocol described in detail by Xu and Webb.[46] The experimental protocol allows prevention of the contribution from linear nonresonant absorption or from excited absorption that is known to lead to artificially enhanced "effective" TPA cross sections when measurements are conducted in the nanosecond regime. TPEF measurements were calibrated relative to the absolute TPEF action cross section determined by Xu and Webb for fluorescein in water (pH = 11) in the 690−1000 nm range. The experimental uncertainty amounts at most to ±10%.

Time-Resolved Fluorescence Anisotropy Measurements. The sample solution was excited with frequency-doubled light from a mode-locked Ti-sapphire laser (Tsunami, Spectra Physics). This produces pulses of approximately 100-fs duration in a wavelength range of 385−430 nm. The polarization of the excitation beam for the anisotropy measurements was controlled with a Berek compensator. The horizontally polarized fluorescence emitted from the sample was up-converted in a nonlinear crystal of β-barium borate using a pump beam at about 800 nm that was first passed through a variable delay line. This system acts as an optical gate and enables the fluorescence to be resolved temporally with a time resolution of about 200 fs (pump-excitation 800/400 nm cross correlation function had a fwhm of 180 fs).[27,33,34,47,48] Spectral resolution was achieved by dispersing the up-converted light in a monochromator and detecting it by using a photomultiplier tube (Hamamatsu R1527P).

Photon Echo and Pump−Probe Measurements. Three-pulse photon echo experiments were carried out with a cavity-dumped Kerr lens mode-locked Ti-sapphire laser pumped by a frequency doubled YVO laser (Millennia, Spectra Physics).[41] The cavity-dumped laser pulse had a duration of 19 fs. The pulse spectrum was centered at ~830 nm. The cavity-dumped beam was focused into a 0.5-mm BBO crystal to convert the fundamental beam into the second harmonic at ~415 nm. Unless mentioned otherwise, the pulse repetition rate was fixed at 38 kHz.

In the 3PEPS experiment, both echo signals at phase-matching conditions $k_1 - k_2 + k_3$ and $-k_1 + k_2 + k_3$ are simultaneously recorded while the time period τ between the pulses 1 and 2 is scanned. Half of the distance between the intensity peaks of these two signals is called "peak shift" which is the essential quantity deduced from the experiment. Thus, the echo peak shift is obtained from the echo profiles and then recorded as a function of population period T between the second and the third pulse. The third pulse creates the superposition state, which may lead in case of a proper phase evolution to the photon echo formation. Photon echo peak shift is sensitive to the extent of the correlation of the phase evolution between the first and the second coherence periods, which is, in turn, sensitive to the transition frequency dynamics during the population period. In our setup three beams of equal intensities (~0.5 nJ per pulse in one beam at the sample) were generated with the aid of thin beam splitters (1-mm-thick quartz substrate, CDP). One pulse (k_1) traveled a fixed delay, whereas the other two pulses (k_2 and k_3) traveled variable delays formed with retroreflectors mounted on DC-motor-driven delay stages (Newport ILS100CCHA) controlled via a Newport ESP7000 motion controller. The three beams were aligned after the delay stages to form the equilateral triangle beam geometry (8-mm sides) and were focused into the 440-μm quartz sample cell using thin singlet lens (f = 18 cm). The two third-order nonlinear signals into the $k_1 - k_2 + k_3$ and $-k_1 + k_2 + k_3$ phase-matching directions were spatially filtered and directed to two photomultipliers (Hamamatsu Photo Sensor Modules H6780). The electrical signals from photomultipliers were measured by two lock-in amplifiers (Stanford Research, SR830), which were referenced to the chopper (SR540) inserted in the k_1 beam. Many measurements were performed in order to confirm reproducibility of the signal. Special attention was paid to the residual peak shift value. The uncertainties of the peak shift value can be estimated at approximately ±0.5 fs over the entire population period up to 100 ps.

In a degenerated pump−probe measurement, only two beams were used, and a neutral density filter attenuated the intensity of the probe beam by a factor of 10 relative to that for the pump beam. The polarization of the probe beam for the anisotropy measurements was controlled with a Berek compensator. The photodiode (ThorLabs DET110) connected to the lock-in-amplifier was used as a detector of the probe beam in pump−probe experiments.

The absorption spectra of the samples were checked before and after data collection, and lack of the observable changes suggests that little or no dendrimer photodegradation or undesired chemical reactions occurred during the measurement.

Numerical Simulations and Fits. In order to derive important spectroscopic parameters from the 3PEPS profile, we performed numerical modeling of the echo signal. We started from a model for the transition frequency correlation function $M(t)$ for a two-level chromophore coupled to the environment and to its own fluctuating nuclei:

$$M(t) = \frac{\langle \delta\omega(0)\, \delta\omega(t) \rangle}{\langle \delta\omega^2 \rangle} \tag{1}$$

where $\Delta\omega(t)$ is the fluctuating part of the electronic transition frequency for each chromophore relative to its central frequency $\langle\omega\rangle$. The quantity $M(t)$ can be used for the description of the memory of the electronic transition frequency and system dynamics when the characteristic frequencies of transition frequency fluctuations are small compared to kT.[49] This high-temperature approach can be applied to describe the coupling of the electronic transition to many intermolecular (solvation) modes at room temperature. The main spectroscopic signals can be most conveniently derived from the complex line shape function $g(t)$:

$$g(t) = P(t) + iQ(t) = \langle \Delta\omega^2 \rangle \int_0^t \mathrm{d}t_1 \int_0^{t_1} \mathrm{d}t_2 M(t_2) + i\lambda \int_0^t \mathrm{d}t_1 M(t_1) \tag{2}$$

or it can be also expressed in terms of spectral density $C(\omega)$:[48]

$$g(t) = \int_0^\infty \mathrm{d}\omega \, \frac{1 - \cos(\omega t)}{\omega^2} \coth\left(\frac{\hbar\omega}{kT}\right) C(\omega) + i \int_0^\infty \mathrm{d}\omega \, \frac{\sin(\omega t)}{\omega^2} C(\omega) \tag{3}$$

In eq 3 $P(t)$ and $Q(t)$ are the real and imaginary parts of $g(t)$, $\langle \Delta\omega^2 \rangle$ is the coupling strength (fluctuation amplitude), λ is the reorganization energy. The absorption spectrum of the system can be calculated by taking the real part of the Fourier transform of $\exp[-g(t)]$:[48]

$$\sigma_a \propto \int_{-\infty}^{\infty} \mathrm{d}t \, \exp[-i(\omega - \langle\omega\rangle)t] \exp[-g(t)] \tag{4}$$

while the third-order photon echo signal in the impulsive limit can be expressed by:[49−51]

$$S_{PE}(\tau,T) \propto \int_0^\infty dt \exp[-\sigma_{inh}^2(t-\tau)^2] \exp\{-2[P(\tau) - P(T) + P(t) + P(\tau+T) + P(T+t) - P(\tau+T+t)]\} \cos^2[Q(T) + Q(t) - Q(T+t)] \quad (5)$$

where σ_{inh} represents the width of the static inhomogeneous distribution.

The peak shift value (position of the maximum, τ_p) was calculated from photon echo signal $S_{PE}(\tau,T)$ as a function of population period T. As the calculation of the echo profile in case of finite pulse width took too much computer time, most of the fitting and modeling procedures were performed in the impulsive limit. The effect of the finite pulse width was estimated by convoluting the pulse electric field envelope (which was taken to be of Gaussian shape with $\sigma = 35$ fs) with the response functions with proper time ordering[50−53] at several population periods (T points), comparing the 3PEPS values with those obtained in the impulsive limit. The ratio $3PEPS_{conv}/3PEPS_{inpuls}$ was weakly dependent on the population period T (at least for some particular important range of interaction strengths and correlation function decay times), and we corrected the impulsive limit results by this factor.[41,50,54] To avoid the canceling effects which can result from using too many parameters, we have attempted to limit the various contributions to $M(t)$ to three exponentials, one constant (static disorder), and one Brownian oscillator in some cases. In effect, the Brownian oscillator contribution qualitatively represents a sum of several intramolecular vibrational modes, which are not exactly known for this dendrimer. Once a set of parameters is obtained, which reproduces the peak shift satisfactorily, the absorption spectrum was calculated and compared with that of the experiment. The initial guess of the energy gap correlation function $M(t)$ can be obtained so that beyond the pulse overlap time interval, the experimental 3PEPS-profile follows $M(t)$ pretty closely.[50−52]

3. Results and Discussion

Linear Spectroscopy. The normalized steady-state absorption and emission spectra of the structures are shown in Figure 1. Steady-state measurements were performed in dilute toluene solutions ($\sim 10^{-6}$ M). The position of the main peak in both absorption and emission shows a bathochromic shift with increasing the dendrimer generation number. This shift is less pronounced in the absorption spectra of **G0**−**G2** as compared to that in fluorescence spectrum. On the other hand for dendrimers larger than **G1** the emission spectrum does not experience any further detectable shift. It seems that the saturation value for the energy of the lowest excited state is reached for the number of linear blocks (segments) in the dendrimer **G1** (9). It is also seen from Figure 1 that there is a drastic difference between the spectra of model linear block **LB** (absorption and emission) and those of the trimer **G0**. The absorption spectrum of **LB** closely resembles that of tolane,[55−57] which is the linear connector used in these dendrimers. The **LB**s spectrum is shifted to the red by ~64 nm with respect to tolane's absorption spectrum due to the lone electron pair of nitrogen atoms (mesomeric effect).[58] The vibronic structure in the absorption spectrum of **LB** is less resolved as compared to that for tolane, but vibronic progressions still can be estimated as very similar to those observed for tolane.[55−57] The absorption spectrum for the trimer **G0** (which is actually formed from three **LB**s) differs drastically from that for **LB**: it is red-shifted by about 3000 cm^{-1} (in addition to the nitrogen lone pair effect in **LB**), and the line shape is also different. This is an indication of strong interbranch coupling and most probably strong electronic correlations through the branching nitrogen center, so the excitation extends beyond the linear (**LB**) unit as was observed for many other nitrogen-cored trimers.[1,2,5,6,27,33,47,48] The fluorescence spectrum of **G0** is also shifted to the red with respect to the fluorescence spectrum of **LB** by approximately the same amount as for the absorption spectrum shift. It is well-established that for small branched molecules possessing charge-transfer character of the excited state the emitting state is localized on a single branch which is accompanied by the breaking of the molecular symmetry.[6,59−64] This scenario of excitation localization on one single branch is not directly applicable to the current dendrimer system as the fluorescence spectra are very different for **LB**, **G0**, and **G1**. However, it does not necessarily imply that the fluorescent (relaxed) state is localized over the same domain as the absorbing state: the extent of delocalization still can be changed as a consequence of nuclear (conformational) relaxation.[65,66]

The photophysical characteristics of dendrimers **G0**−**G2** are summarized in Table 1. All peak molar extinction coefficients are high. The peak extinction ϵ_{max} has been found to be nearly proportional to the number of branches (Table 1). The oscillator strength of the absorbing transition (~extinction integrated over the absorption line) also increases nearly linearly with the number of branches (not shown). It is immediately seen from Table 1 that all of the dendrimers in this series exhibit a high fluorescence quantum yield exceeding 0.7 and small Stokes shifts as compared to those of other known large conjugated dendrimers.[27−32,67]

Analysis of the fluorescence lifetimes obtained by time-correlated single-photon counting measurements and fluorescence quantum yield measurements resulted in relatively short spontaneous radiative lifetimes for fluorescent states, which is in turn an indication of high strength of the respective electronic transitions (Table 1). We estimated emission transition dipole moments of dendrimers using the known expression for the Einstein A coefficient:[68]

$$\mu_{em}^2 = \frac{3\hbar}{32\pi^3 \nu_{em}^3 n \tau_{Rad}} \quad (6)$$

where c = speed of light, n = refractive index, $\epsilon(\nu)$ = the molar extinction coefficient in M^{-1} cm^{-1}, at the wavenumber ν, in cm^{-1}, and

$$\frac{1}{\nu_{em}^3} = \frac{\int \nu^{-3} F(\nu)}{\int F(\nu)} d\nu, \quad F(\nu) = \text{fluorescence spectrum}$$

All of these findings (high quantum yields, large emission transition dipole moments comparable with those for absorbing states, small Stokes shifts) suggest a relatively small reorganization of the excited state during its evolution to the emission state, even for large dendrimers. This is in sharp contrast with the phenylacetylene (compact) dendrimers family (based on the same tolane connector, with benzene as the branching center) where the spectroscopic properties of the excited-state configuration were found drastically different from those for the ground-state configuration.[31,69] Transition dipole moments associated with absorption bands can be formally calculated as a square root of the extinction coefficients integrated over the absorption band.[68] This procedure gave us 14.5 D, 25.6 D, and 37.2 D for **G0**, **G1**, and **G2** respectively. However, this procedure of evaluation of the transition dipole moment implies that overall absorption band is due to a single electronic transition, whereas the absorption band for the dendrimers showed

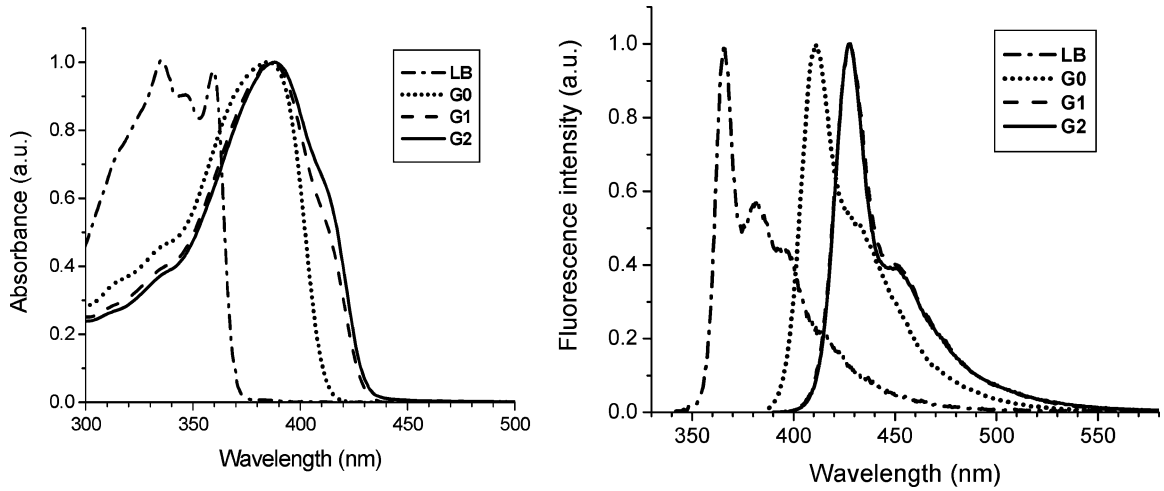

Figure 1. Normalized absorption and fluorescence spectra of the dendrimers **G0**, **G1**, **G2** as well as of the linear structure **LB**.

TABLE 1: Photophysical Parameters for the Dendrimers G0−G2 in Toluene

	λ_{abs} (nm)	ϵ_{max} ($M^{-1}\cdot cm^{-1}$)	λ_{em} (nm)	Stokes shift (cm^{-1})[a]	Φ_F[b]	τ_F[c] (ns)	τ_{Rad}[d] (ns)	μ_{em}[e] (D)
G0	385	115000	411	1634	0.77	0.88	1.14	11.38
G1	387	347000	427	2421	0.74	0.71	0.96	13.23
G2	388	811000	427	2354	0.72	0.70	0.97	13.15

[a] Stokes shift $= (1/\lambda_{abs} - 1/\lambda_{em})$. [b] Fluorescence quantum yield in toluene determined relative to fluorescein in 0.1 N NaOH. [c] Experimental fluorescence lifetime measured by time-correlated single-photon counting (TCSPC). [d] Radiative lifetime $= \tau_F/\Phi_F$. [e] Emission transition dipole moment estimated from the radiative lifetime (see text eq 6).

spectral details (Figure 1a) which are most probably related to the presence of several overlapping transitions. This is not surprising for these large macromolecules composed of up to 21 chromophores. It is also known that for aggregated multichromophoric systems the linear absorption spectroscopy is insensitive to the exciton delocalization length and the calculated transition dipole simply reflects the additive extinction of all chromophores comprising the aggregate.

In an attempt to better understand the structure of the spectroscopic transitions we also performed a decomposition of absorption and fluorescence spectra of **G0**−**G2** into Gaussian components (into three components for absorption and into two components for fluorescence spectra) using best-fit procedures. All fluorescence spectra showed the same separation between two Gaussians (∼1115 cm^{-1}) which is a strong indication of the vibronic progression. Most probably it is associated with the N−C stretching mode (∼1200 cm^{-1}) and/or the benzene ring distortion mode similar to that observed in tolane (996 cm^{-1} in the gas phase,[57] ∼1000 cm^{-1} in solution[56]). The main fluorescence peak is quite narrow for all samples (Gaussian width $w = 697-758$ cm^{-1}), and its width has a tendency to decrease when the dendrimer size (generation number) increases.

Figure 2 shows this dependence on generation number as well as the example of the decomposition of the **G2**-fluorescence spectrum into Gaussian components. The trend of narrowing the fluorescence spectrum is quite remarkable because one can expect higher disorder and increased degrees of freedom leading to the line broadening. For the absorption transitions of **G0**−**G2** the structure in the spectra is less pronounced as compared to that in fluorescence spectra, and a single vibronic progression is not so clearly seen there. This can be an indication of several overlapping electronic (excitonic) transitions forming absorption spectra. It is worth noting that in spite of the not so pronounced structure in the trimer's (**G0**) absorption spectrum at least three Gaussians are necessary for any reasonable fit, and a low-energy Gaussian component was always found to have a similar but slightly larger width as compared to that of the main component in the fluorescence spectrum (880 ± 75 cm^{-1} vs 760 ± 10 cm^{-1}). The same trend is also seen for **G1** and **G2** (756 ± 35 cm^{-1} vs 741 ± 6 cm^{-1} and 783 ± 35 cm^{-1} vs 697 ± 6 cm^{-1}, respectively). The trend of the narrowing of this component with the increase of the dendrimer size is less marked for the absorption than for the fluorescence spectrum (Figure 2), but obviously there are no signs of broadening with the rise of the generation number. The shift to lower transition energies with increasing generation number was found for all decomposition components. This red-shift combined with the line narrowing for larger dendrimers discussed above could be a signature of the delocalization of the excitation beyond the trimer configuration. However, more proof from time-resolved and nonlinear optical experiments is necessary.

Two-Photon Absorption. TPA cross sections were measured by the two-photon excited fluorescence method in the femtosecond regime (see Experimental Section) and are summarized in Table 2. It is seen that there is a strong enhancement over the additive behavior when going from the trimer (**G0**) to higher generations (**G1** or **G2**). TPA-cross sections given in Table 2 have been taken at 740 nm, which is not exactly the wavelength at the peak of two-photon absorption spectrum for all generations, but it gives a good indication of the relative magnitude of the TPA response of the different dendrimers. A value of up to 7000 GM was obtained for the largest dendrimer at the maximum.[70] More detailed investigation of TPA spectra will be published elsewhere.[70] Here we mention that the trends described here are similar to those for the TPA cross sections taken at peak TPA wavelengths.[70] This is irrespective of the scaling used for the macromolecules size (i.e., the number of linear building blocks, the number of effective π-electrons, or the number of branching centers.[3−5,71]) Contrary to the behavior of conjugated dendrimers with different branching centers,[72] a major increase of the normalized TPA (σ_2/N_e[71]) is observed from the trimer **G0** to the dendrimer **G1**. Also, although the absolute TPA cross sections for the trimer compound **G0** are lower than those of its stilbenyl analogue,[28,32] the striking difference is a much stronger increase of the normalized TPA in dendrimers **G1** and **G2** in the investigated series, suggesting the importance of the nature of the building blocks and branching centers in the delocalization process.

Time-Resolved Spectroscopy. It is known that time-resolved fluorescence anisotropy experiments can provide valuable

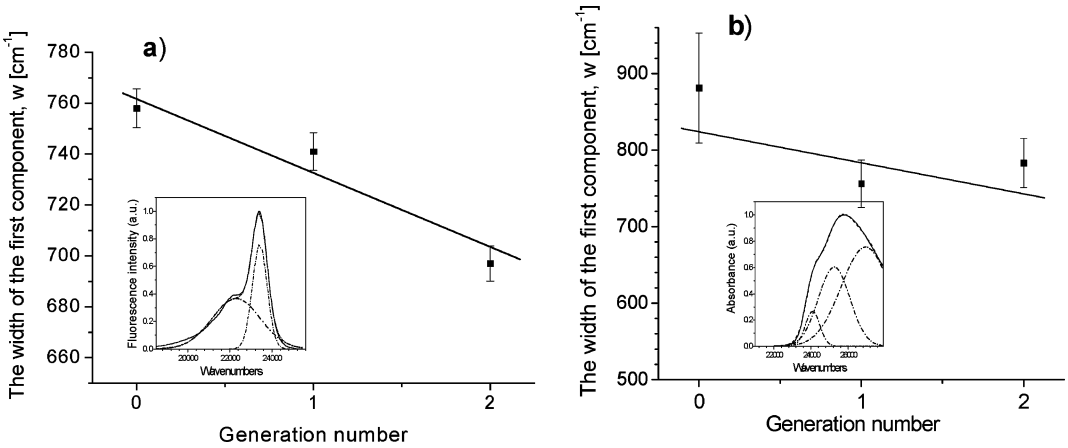

Figure 2. Dendrimer size dependence of the Gaussian component width *w*. (a) Main Gaussian component of the fluorescence spectrum, (b) low-energy Gaussian component in the absorption spectrum. Straight lines are guides for eye. (Insets) Examples of the decomposition into Gaussian components for **G2**.

TABLE 2: Two-Photon Absorption Data for the Dendrimers G0−G2 in Toluene

	λ_{abs} (nm)	ϵ_{max} (M^{-1}·cm^{-1})	$\mu_{em}a$ (D)	σ_2(GM)[b]	σ_2/N_e(GM)[c]
G0	385	115000	11.38	32	1.3
G1	387	347000	13.23	370	8.8
G2	388	811000	13.15	840	13.1

[a] Estimated from the radiative lifetime (see text eq 6). [b] 1 GM = 10^{-50} cm^4·s·$photon^{-1}$; TPEF measurements were performed using a mode-locked Ti:sapphire laser delivering 80 fs pulses at 80 MHz, calibrating with fluorescein. [c] Two-photon absorption cross section (σ_2) measured at 740 nm normalized by the effective number of π-electrons in the conjugated system N_e (**G0**: 24.2; **G1**: 42; **G2**: 64.2). The effective number of electrons is calculated following the method introduced by M. Kuzyk et al. for comparative analysis of molecules of different topologies including dendrimers.[71]

information about the excitation energy migration and interbranch coupling in branched molecular systems.[1,2,5,47,48] By utilizing fluorescence depolarization it is possible to follow the intramolecular excitation transfer.[1,2] Similar information can be obtained by pump−probe spectroscopy, but these results can be severely complicated by a contribution of the polarized excited-state absorption with complex dynamics.[64] Anisotropy decay results for large dendrimer systems (e.g., **G2**) on different time scales are shown in Figure 3. Experimental fluorescence anisotropy $R(t)$ was calculated from the decay curves for the intensities of fluorescence polarized parallel $I_{par}(t)$ and perpendicularly $I_{per}(t)$ to the polarization of the excitation light according to the equation:

$$R(t) = \frac{I_{par} - GI_{per}}{I_{par} + 2GI_{per}} \quad (7)$$

The factor G accounts for the difference in sensitivities for the detection of emission in the perpendicular- and parallel-polarized configurations.

Three major time components are immediately seen in the fluorescence anisotropy decay profile. Taking into account the size of **G2** and the viscosity of toluene (∼0.56 cP at 25°) the longest time decay component (or near flat residual anisotropy on 10-ps time scale) is associated with the overall molecular rotation (rotational diffusion) of **G2** in toluene. There is also a very fast decay component which is associated with strong interbranch interaction and formation of the state delocalized over the area larger than one branch.[1,2,27,34,47,48] Fluorescence anisotropy decay on a short time scale is shown in the inset of

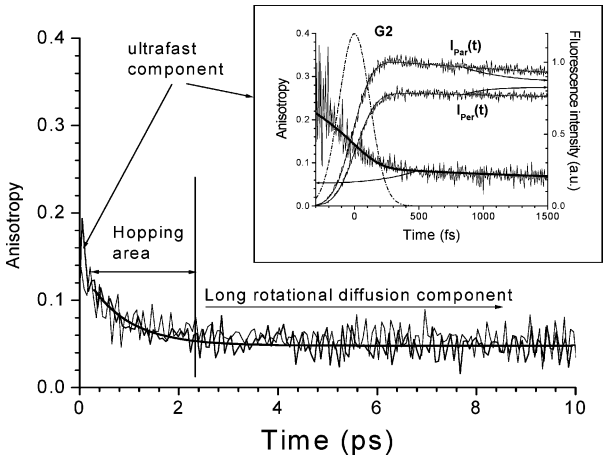

Figure 3. Time-resolved fluorescence anisotropy of the **G2**. Excitation wavelength: 410 nm, emission (detection) wavelengths are 440 nm, 480 nm (undistinguishable within the experimental error). Best fit with the two-exponential function is shown for the **G2**. (Inset) Fluorescence anisotropy dynamics on short time scale for the **G2**. Time-resolved fluorescence components polarized perpendicular and parallel with respect to the excitation are shown on the same graph. Dash−dot line represents the instrument response function for the fluorescence intensity. Best fit to two-exponential anisotropy decay function is also shown (see text for details).

Figure 3. The raw fluorescence anisotropy decays from an initial value ∼0.22 to the residual anisotropy of ∼0.09 within the instrument response function (IRF) duration. However, in case of fast dynamics the measured profiles $I_{par}(t)$, $I_{per}(t)$ are the results of a convolution of the instrument response function with true fluorescence intensity profiles. In this case the raw anisotropy looks different from the true anisotropy profile at short times, and it peaks at negative times. Parameters of true anisotropy decay can be estimated by special best-fit procedures, assuming the convolution of the IRF with model parallel and perpendicular fluorescence intensity profiles.[73,74] The best fit to a two-exponential anisotropy decay model is shown in the inset of Figure 3 by the solid line. The best-fit model anisotropy was found to decay from initial value of 0.40 ± 0.05 with the time constant of 27 ± 10 fs. Such a fast process cannot be described by Förster theory with realistic parameters. This process corresponds to a strong coupling regime and occurs within the spectroscopic unit. Along with the ultrafast 27-fs component and long anisotropy decay associated with rotational diffusion, an additional small picosecond component ($\tau \approx 1$ ps) is also clearly seen in the fluorescence anisotropy decay

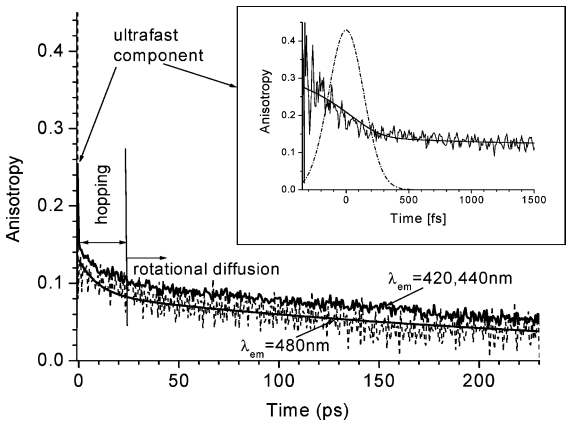

Figure 4. Time-resolved fluorescence anisotropy of the trimer system (**G0**). Excitation wavelength: 390 nm; emission (detection) wavelengths are indicated on the graph. Best fit with the two-exponential function is shown for the $\lambda_{em} = 480$ nm result. (Inset) Fluorescence anisotropy dynamics on short time scale for emission wavelength 480 nm. Dash−dot line represents the instrument response function for the fluorescence intensity (normalized to 0.43). Best fit result with fast exponential anisotropy decay function is also shown (see text for details).

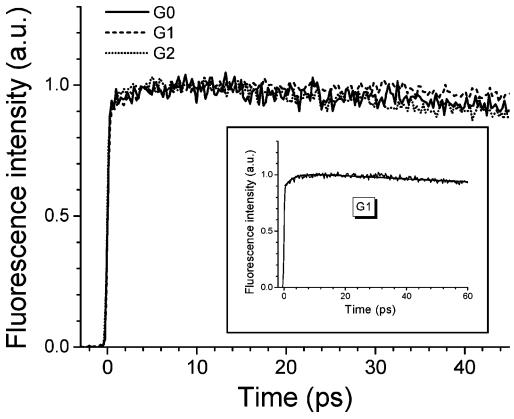

Figure 5. Isotropic (magic angle) fluorescence dynamics of the fluorescence. Best fit to a two-exponential function for G1 is shown in the inset (rise time = 2.93 ps, decay time = 710 ps).

profile (Figure 3). This component is too fast for rotational diffusion. Intermolecular energy transfer can be also ruled out because at the concentration used in this experiment ($c = 10^{-5}$ M) the average intermolecular distance is about 50 nm, while the Förster radius for trimer−trimer energy transfer can be estimated to be a few nanometers (see below). This combination of parameters (including **G2** fluorescence lifetime shown in Table 1) leads to intermolecular energy transfer times on a submillisecond time scale. Therefore, we should assign this 1-ps component in the transition dipole reorientation to the intramolecular (intradendrimer) process. In general, the presence of multiexponential anisotropy decay in a multichromophore system possessing the axial symmetry is an indication of the presence of inhomogeneity in the aggregated system. Intramolecular chromophore clustering associated with disorder can be suggested as a reason for two, distinct, decay time components as it was found for the photosynthetic antenna complex.[75] Fast equilibration within a coherently coupled cluster can result in an initial 27-fs drop in anisotropy, while the remainder of the depolarization (prior to rotational diffusion) can be due to the relatively slow, incoherent, energy transfer between clusters (spectroscopic units).

In order to get more insight in the actual size of the spectroscopic unit in large dendrimers we consider the anisotropy dynamics as a function of generation number. Anisotropy decay results for the smallest dendrimer **G0** (trimer) on different timescales are shown in Figure 4.

Three major time components are also seen in the fluorescence anisotropy decay profile. The size (volume) of **G0** is appreciable smaller than that for **G2**, and the long decay component associated with the rotational diffusion of **G0** in toluene (time constant about 300 ps) is clearly resolved in Figure 4. There is also a very fast decay component which is associated with strong interbranch interaction.[1,2,27,34,47,48] Fluorescence anisotropy decay on a short time scale is shown in the inset of Figure 4. The fluorescence anisotropy decays from an initial value ∼0.2 to the residual anisotropy of ∼0.125 within the instrument response function (IRF) duration. The best fit to the exponential anisotropy decay model is shown in the inset of Figure 4 by the solid line. The best-fit model anisotropy was found to decay from initial value of 0.40 ± 0.05 (see discussion about deconvolution procedure and true initial anisotropy given above) with the time constant of 40 ± 10 fs. This fast decay along with the spectral changes from the monomer to the trimer suggests a strong coupling regime in the trimer. If we formally apply a phenomenological model developed by Leegwater[76] for the aggregate of three chromophores as we did for some other trimer systems,[27,48] we can see immediately that it is not possible to have anisotropy decay $\tau_R = 40$ fs and to reside in the Förster (hopping) regime.[48] This model also indicates the effective interbranch coupling strength J exceeding 1000 cm^{-1} for $\tau_R =$ 40 fs and the line width of **G0**. This effective interaction strength is in qualitative agreement with the apparent red-shift of absorption spectrum peak from the monomer to the trimer (∼3000 cm^{-1}). While Leegwater's model can give a qualitative picture, great care should be taken in applying this model for quantitative analysis of the excitation dynamics in **G0**. Dramatic spectral change from the monomer **LB** to the trimer **G0** (Figure 1) suggests strong electronic correlations through the nitrogen, and most probably, the system cannot be considered as an aggregate of three individual chromophores with electron−hole pairs localized on individual branches (Frenkel excitons). Along with the ultrafast 40-fs component and long anisotropy decay associated with rotational diffusion (∼300 ps), the additional small picosecond component ($\tau \approx 9$ ps) is also clearly seen in the fluorescence anisotropy decay profile (Figure 4). Similar to **G2** this component can be assigned to the hopping between spectroscopic units. The residual anisotropy before rotational diffusion starts was found to be fluorescence-wavelength dependent, which is not the case for the homogeneous planar trimer system. This is an indication of the presence of inhomogeneity in the system. We can suggest that due to some conformational disorder (most probably due to the twisting around the triple bond) the excitations are not delocalized over the entire trimer for some fraction of the **G0** molecules, thus leaving the space for intramolecular hopping process in this subensemble. Similar behavior was reported in amino-substituted phenylbenzene derivative.[59,60] In these experiments the contribution of the picosecond (∼6 ps) component in polarization dynamics was observed along with a relatively low initial anisotropy (∼0.16), most probably associated with unresolved ultrafast component.[59] A photon echo experiment (which we will discuss below) directly confirms the presence of static inhomogeneous broadening for **G0** in solution.

The isotropic (magic angle) time-resolved fluorescence was found to be similar for all generations, and it showed no fast dynamics on the picosecond and subpicosecond time scale (Figure 5). A weak rise-time feature seen in Figure 5 was found

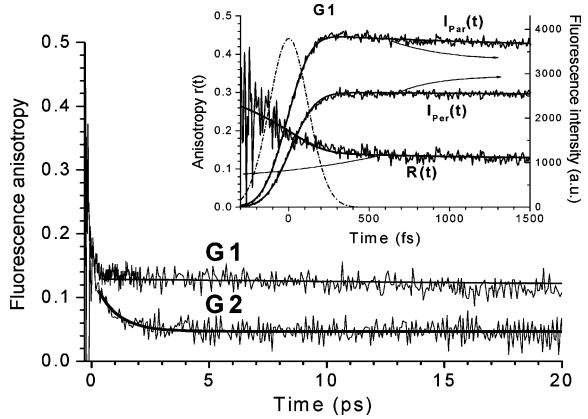

Figure 6. Time-resolved fluorescence anisotropy of the **G1**, **G2**. Excitation wavelength = 410 nm; emission (detection) wavelengths = 440 nm. Best fit with the two-exponential function is shown for the **G2**. (Inset) Fluorescence anisotropy dynamics on short time scale for the **G1**. Time-resolved fluorescence components polarized perpendicular and parallel with respect to the excitation are on the same graph. Dash−dot line represents the instrument response function for the fluorescence intensity. Best fit to exponential anisotropy decay function is also shown (see text for details).

to be emission-wavelength dependent in a way typical for the solvation effect.[77]

Comparison of the fluorescence anisotropy decay for **G1**, **G2** is presented in Figure 6. The rotation diffusion time for large molecules **G1**, **G2** is expected to be longer than for **G0**, and the corresponding long-time anisotropy component is not seen on the time scale of Figure 6. Similar to that for **G0**, **G2** the anisotropy for **G1** drops down rapidly to the level near ∼0.12, indicating strong interbranch coupling. The short time-scale profiles for the anisotropy of **G1** and polarized fluorescence components are shown in the inset as well as the best-fit curves. Best-fit results gave the initial anisotropy near 0.4 and the fast anisotropy decay component of 35 ± 10 fs for **G1**.

Such a fast process cannot be described by Förster theory with realistic parameters. This process corresponds to strong coupling regime and occurs within the spectroscopic unit. The most important feature of the anisotropy dynamics of **G1**, **G2** is the absence of a picosecond (hopping) component for **G1** and the reappearance of this component in the anisotropy profile of **G2**. From the steady-state spectra (Figure 1) and the related discussion it is seen that the spectroscopic units for **LB**, **G0**, and **G1** are different. However, it is not clear whether the size of this domain can exceed the trimer configuration. The absence of a hopping component for **G1** indicates that spectroscopic unit in this dendrimer is comparable with the size of **G1**, and no room for hopping is left. For **G2** the anisotropy associated with the hopping process starts decaying from the same value at which the ultrafast decay process in **G1** has completed and results in appreciably lower residual anisotropy than for **G1** at longer times apparently due to the larger variety of accessible dipole orientations in **G2**. It is interesting to compare the hopping time scale in **G2** with that observed in the trimer **G0**. Best-fit results showed substantially faster hopping-associated anisotropy decay for **G2** (≅1 ps) as compared to that for **G0** (≅9 ps). This again indicates very different spectroscopic units in these two systems. It is interesting to compare the fluorescence anisotropy results with those of polarized degenerate pump−probe experiment.[78] If not strongly affected by an excited-state absorption, this experiment provides information about depolarization taking place in the excited state due to equilibration between degenerate or near degenerate states (as opposed to the energy-relaxed (Stokes-shifted) states in fluorescence). The pump−probe anisotropy decay result is shown in Figure 7.

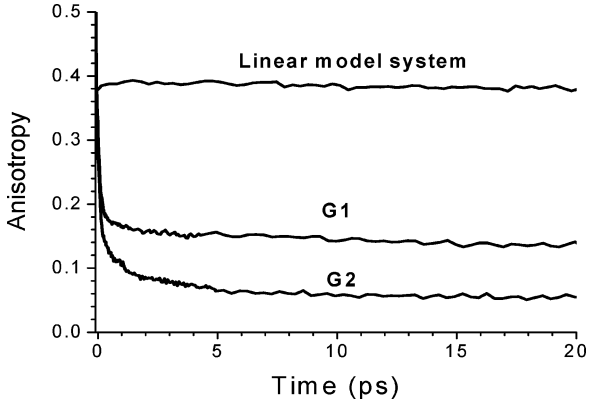

Figure 7. Time-resolved pump−probe anisotropy of the **G1**, **G2**. Pump and probe wavelength = 412 nm. The anisotropy profile for the model linear system is also shown for comparison.

Although decaying to slightly higher residual values, the pump−probe anisotropy demonstrated a remarkably similar behavior to that for fluorescence anisotropy. It strongly suggests that fast transition moment reorientation is not essentially associated with downhill energy relaxation but rather takes place during the equilibration between near isoenergetic states and due to the dephasing process.[79,80] This is an important finding characterizing the Frank−Condon configuration which is important for the TPA process. The fast anisotropy component in these degenerate pump−probe signals strongly suggests a delocalized state in the "hot" nonrelaxed configuration of the system. The presence of an ultrafast component of the anisotropy decay strongly supports the idea of a coherent strong interbranch coupling regime in these dendrimers. It is also interesting to compare anisotropy decay times in large dendrimers with those predicted by Förster theory for trimer−trimer energy transfer. The Förster radius calculated using the overlap of the absorption and emission spectrum of the **G0** was found to be $R_F = 30.96$ Å. The distance between two adjacent trimer blocks in the dendrimer R_{DA} can be calculated from molecular structure as 21.7 Å. Using the well-known relation

$$k_t = \frac{1}{T_D}\left(\frac{R_F}{R_{DA}}\right)^6 \tag{8}$$

(T_D = **G0** lifetime, k_t = energy transfer rate) we arrive at the transfer time 112 ps, which is much longer than the observed hopping time in **G2** (≅1 ps). Although this is a rough estimate (point-dipole approximation is used, which is not well justified in this tight system), it remains obvious that the trimer-like spectroscopic units interacting via the Förster mechanism cannot explain the hopping component of energy migration between spectroscopic units in a large dendrimer. The spectroscopic unit seems to be different from that of the simple trimer, and as previous analysis showed, it is comparable in size with **G1**, thus exceeding the trimer configuration.

Photon Echo Spectroscopy. Another parameter affecting the spectroscopic unit in the larger-generation dendrimers is in regards to the nature of interaction with solvent and line broadening mechanisms. Three-pulse photon echo peak shift (3PEPS) spectroscopy is known to be sensitive to these interactions.[50−52,54,81,82] In the photon echo experiment the laser pulse is split into three equal energy pulses (aligned in an equilateral triangle geometry in our case, Figure 8). Two pulses

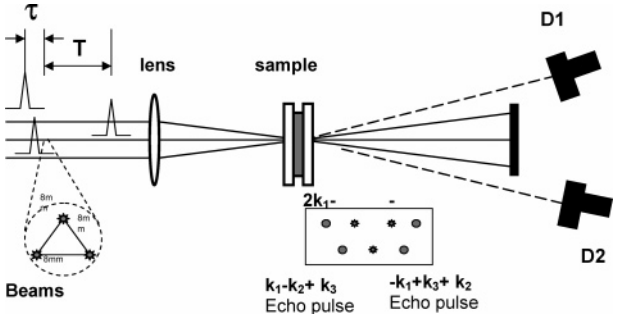

Figure 8. Spatial configuration and phase matching diagram for the photon echo experiment.

travel over variable delay lines, providing the two experimentally controllable time periods: the coherence period, which is the time delay between the first and second pulses, and the population period, which is the time delay between the second and third pulses. In the 3PEPS experiment, both echo signals at phase-matching conditions $k_1 - k_2 + k_3$ and $-k_1 + k_2 + k_3$ are simultaneously recorded, while the time period τ between the pulses 1 and 2 is scanned (Figure 8). Half of the distance between the intensity peaks of these two signals is called "peak shift" which is the essential quantity deduced from the experiment. The pulse duration was estimated to be 46 fs at the sample cell (see Experimental Section for the details). In addition to the valuable information about the energy gap fluctuations, which can be obtained from the echo peak shift (it will be discussed below), the integrated echo signal intensity can also provide an important piece of information about transition moment scaling. Under the same excitation conditions and equal sample optical densities the three-pulse echo signal intensity scales as $\sim(\mu_{ge}^8)$,[83] (μ_{ge} transition dipole moment in absorption configuration). As we have mentioned above, the linear spectroscopy is not able to provide us with the true value of the absorbing transition dipole moment (or the extent of delocalization) for large multichromophoric molecules or molecular aggregates. Different nonlinear methods were applied to evaluate the transition dipole moment or coherent domain size scaling in organic macromolecules or aggregates such as absorption saturation,[66] third harmonic generation,[84,85] or two- and three-photon absorption.[32] The resonance four-wave mixing signal amplitude provides a very steep dependence on the transition dipole moment which can be used to follow the absorbing-state transition dipole moment trend as a function of generation number. Figure 9a shows the three-pulse photon echo signal intensity as a function of the dendrimer size (generation number). The dependence of the emission-state transition moment on the dendrimer size calculated using eq 6 is given for comparison in Figure 9b. Although the first graph reflects the trend in the absorbing transition dipole and the second one shows the trend in emission transition, both graphs suggest the rise of spectroscopic unit size when going from the trimer configuration to **G1** and near similar parameters for **G1** and **G2**. The TPA cross section normalized to the number of effective π-electrons which can also serve as a measure of coherent domain[28,32] is shown in Figure 9c. This result indicates the domain size being larger than or comparable to the size of **G1**. These findings are in accordance with the time-resolved anisotropy results reported above.

As we mentioned above, the echo peak shift is obtained as half of a distance between two echo profiles detected in two phase-matching directions and then recorded as a function of population period T between the second and the third pulse. The peak shift reflects the rephasing and echo formation capability of the medium. During the population period T the system is in a diagonal population state, and thus the peak shift decay reflects processes that cause the transition frequency changes within the spectral window of the laser pulse. The echo peak shift method is capable of providing time scales and coupling strengths of dephasing processes that are coupled to electronic transition by providing a line shape function and separating the static contribution to the line broadening.[50−52,54,81,82] The theoretical treatment of the third-order nonlinear optical signals for the two-level system with linear electron phonon coupling has been described elsewhere.[49] Although using the two-level system with linear electron−phonon coupling to model the chromophore-bath system is sometimes an oversimplification when applied to complex macromolecular systems, many new findings about excitation energy transfer and contributions of static disorder, time scales, and coupling strengths to the bath were made using the 3PEPS-method, and this approach was used for natural photosynthetic antenna complexes,[86−89] *J* aggregates,[90,91] chromophore-labeled antibody binding sites,[92,93] and polymers.[37,81] Our previous measurements with three-pulse photon echo spectroscopy with a monomer, dimer, and trimer system showed the trimer has a smaller interaction with the environment, which can be rationalized by delocalization in the branched structure.[1,2,41]

Although not straightforward in modeling and interpretation, 3PEPS can provide unique information such as the contribution of static disorder in solutions and time scales of transition-coupled nuclear motions on extremely wide time scales which is hard to obtain by other spectroscopy methods. Combining 3PEPS with other techniques helps us to build up a consistent comprehensive picture of line broadening and energy migration mechanisms in molecular systems. Representative integrated three-pulse photon echo signals for **G2** at $T = 0$ fs, $T = 133$ ps are shown in Figure 10.

It is seen that the peak shift decreases as T increases and there is nonzero residual peak shift at 133 fs. Initial peak shift is quite high (~27 fs, 25 fs for **G0**, **G1**, exceeds 25 fs for all generations) which is comparable with that reported for the natural photosynthetic systems[86−89] and *J* aggregates.[90,91] While the initial peak shift can be affected by the laser pulse duration,[50−52] it reflects in our case a relatively weak coupling to the bath for the dendrimers, which is in accordance with the relatively small Stokes shift measured by steady-state spectroscopy (Figure 1). It is worth noting that dendrimers were excited to the red of the absorption maxima (the excitation laser pulse spectrum peaked at 409 nm for **G0** and 413 nm for **G1**,**G2**). This mode of excitation helps to minimize contribution from high-frequency vibrations and overtones to the signal.[94,95] Comparison of the 3PE peak shift decay for **G0** and **G1** on two time scales is shown in Figure 11. It is clearly seen from this figure that the 3PEPS decay profile for the trimer **G0** is different from that for **G1**. This means that the fluctuations that are coupled to electronic transition are different for each of these two dendrimers. Simulated data are indicated by solid lines (see details below).

The initial peak shift decay is faster for **G1** as compared to **G0** while the picosecond component is faster and has larger amplitude for **G1**. It is likely that the picosecond time scale arises from a weakly polar solvation effect in toluene.[96] This is a bath response to changes in geometry of the probe chromophore when excited. 3-ps and 0.6-ps solvation components were found for the small-probe chromophore in toluene.[96] Our isotropic time-resolved fluorescence measurements also showed rise-time constant of ~2.9 ps (see Figure 5), which can be

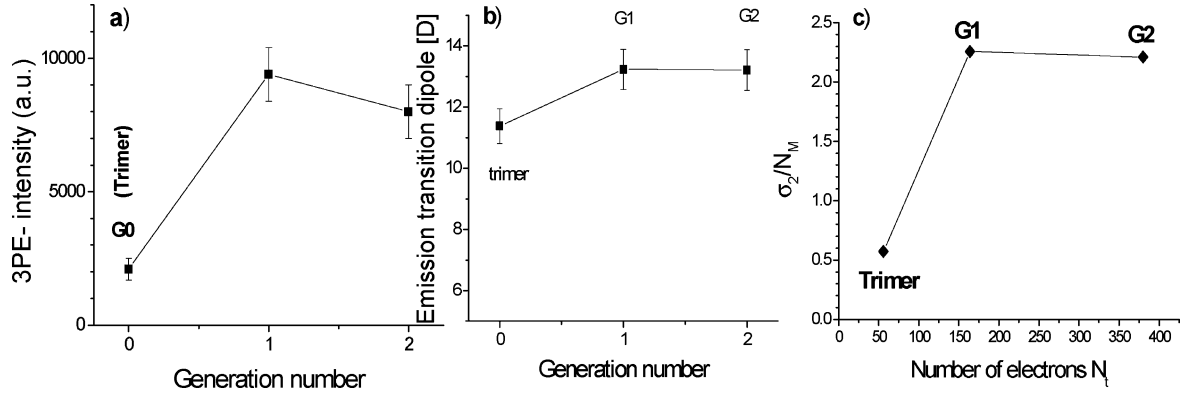

Figure 9. Photon echo intensity (a), emission transition moment (b), and normalized TPA cross section (c) as functions of the dendrimer size.

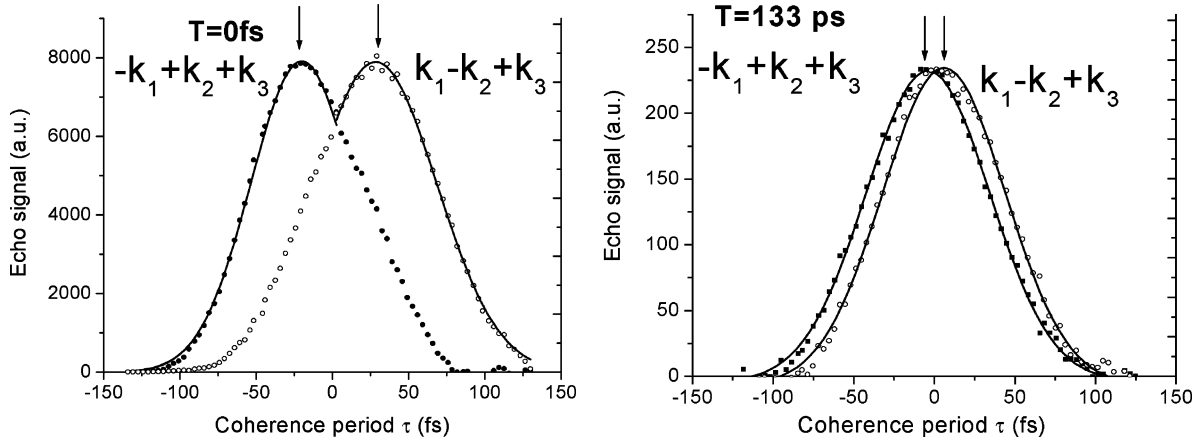

Figure 10. Representative integrated three-pulse photon echo scans for **G2**: (a) population period $T = 0$ fs, (b) population period $T = 133$ ps. Phase matching directions for the data are indicated on the graphs. The solid lines represent the Gaussian fit of the echo data. The echo peak shift is obtained as a half a distance between two echo profiles (indicated with arrows).

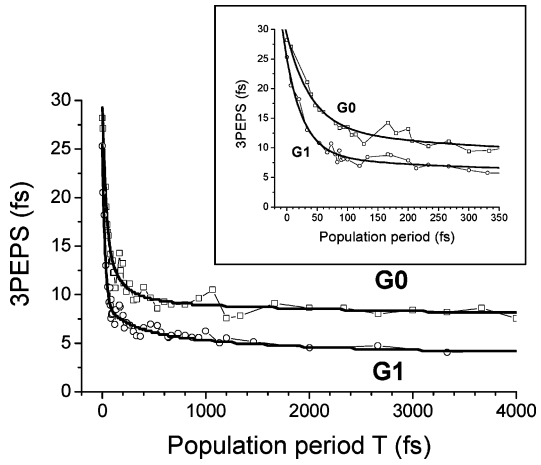

Figure 11. Three-pulse photon echo peak shift for dendrimers **G0**,**G1** as a function of population period T on medium and short (inset) time scales. Solid lines represent the result of model calculations for medium time sale. Direct fit to multiexponential decay function is shown for the short time scale in the inset.

associated with weak solvation in toluene.). However, 3PEPS numerical modeling suggested different time constants in this range 0.3 ps (**G0,G1**) and 2 ps (**G0**), 6.5 ps (**G1**) (see below). It cannot be ruled out that the latter picosecond components are in fact superposition of several exponentials with close decay times including the solvation component ~3 ps. However, even in this case a relative contribution of the solvation component remains small. It is clear that most of the dephasing in these large macromolecules is associated with intramolecular processes rather than with solvation, similar to what was reported for polymers[38] and *J* aggregates.[90,91] Slowly decaying oscillations in the 3PEPS profile are also seen in the range 80−1000 fs for both **G0** and **G1**. They are due to the coherently excited intramolecular vibrations weakly dumped by the bath, and they are more pronounced for the trimer as compared to those for larger dendrimers. Effective single-frequency vibration modeling came up with the frequency ~155 cm^{-1}, which can be associated with low-frequency torsional motions around the triple bond.[57]

Since we do not know the exact vibronic structure of these large molecules, it is difficult to determine the detailed functional form of $M(t)$. In order to obtain a qualitative picture of the main time scales and coupling strengths to the bath nuclear modes, we performed numerical modeling of the 3PEPS signal using the model correlation function best represented by three exponentials and the offset σ^2_{inh} which is related to the static inhomogeneity: (see the details in Experimental Section and Numerical Simulation section)

$$M(t) = \left[\sum_{i=1}^{3}\langle\Delta\omega_{ei}^2\rangle \exp\left(-\frac{t}{\tau_{ei}}\right) + \sigma_{inh}^2\right] / \left(\sum_{i=1}^{3}\langle\Delta\omega_{ei}^2\rangle + \sigma_{inh}^2\right) \quad (9)$$

where $\langle\Delta\omega_{ei}^2\rangle$ are the coupling strengths, which are related to the reorganization energies $\lambda_{ei} = \langle\Delta\omega_{ei}^2\rangle/2kT$ (k = Boltzman constant, T = temperature) in high-temperature limit.[49] For **G0** we obtained correlation times $\tau_{e1} = 100$ fs, $\tau_{e2} = 300$ fs, and $\tau_{e3} = 6500$ fs, and reorganization energies $\lambda_{e1} = 117$ cm^{-1}, $\lambda_{e2} = 65$ cm^{-1}, $\lambda_{e1} = 169$ cm^{-1}. Relatively high offset in 3PEPS data resulted in static inhomogeneity $\sigma_{inh} = 450$ cm^{-1}. For **G1** static inhomogeneity was found to be substantially smaller σ_{inh}

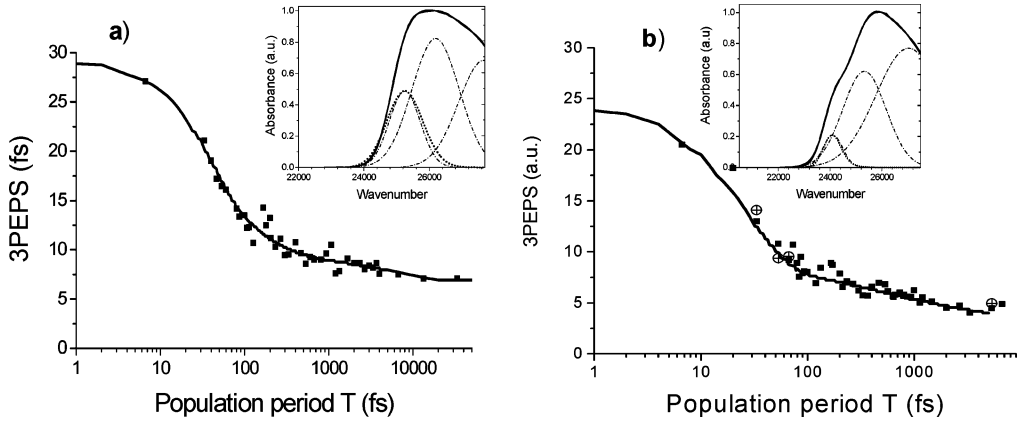

Figure 12. Result of numerical modeling of three-pulse photon echo peak shift (3PEPS) for dendrimers **G0** (a), and **G1** (b**)** as a function of population period *T*. 3PEPS data for **G2** are shown by crossed circles. (Inset) Absorption spectrum decomposed into Gaussian components and the spectrum calculated from model $M(t)$ for the respective dendrimer.

$= 169\ cm^{-1}$ in spite of the larger size of the dendrimer. Correlation times and reorganization energies for **G1** were found from 3PEPS fit to be $\tau_{e1} = 25$ fs, $\tau_{e2} = 300$ fs, and $\tau_{e3} = 2000$ fs, and reorganization energies $\lambda_{e1} = 154\ cm^{-1}$, $\lambda_{e2} = 33.8\ cm^{-1}$, $\lambda_{e1} = 34.3\ cm^{-1}$, respectively. These parameters are different from those for **G0** (except τ_{e2}) indicating different spectroscopic units in these systems. It is also worth noting that there is no increase in the total reorganization energy of exponential components in the larger molecule **G1** with respect to that in **G0** (actually it is slightly smaller for **G1**). Considering the relatively high peak shift values it was not possible to simulate the entire relatively broad absorption spectrum and 3PEPS data using the same correlation function. However, we have obtained a good match for the first spectral Gaussian component discussed above. The results of spectrum simulations using $M(t)$ for **G0** and **G1** are shown in the insets to Figure 11. Although the Gaussian decomposition remains somewhat uncertain, 3PEPS results indicate the presence of a real spectral structure with different electronic transitions under a broad absorption spectrum envelope. Much smaller inhomogeneous spectral broadening and slightly smaller dynamical broadening found for **G1** as compared to the trimer (**G0**) is a strong indication of motional narrowing effect[97,98] due to the larger delocalization length (spectroscopic unit) in **G1** as compared to **G0**, although some contribution from torsion hindering as a result of the "amino-conjugation effect"[99] cannot be ruled out.

Measurements taken at several population periods indicated that 3PEPS for **G2** appeared to follow that for **G1** quite closely (points are shown in Figure 12b); however, more work is necessary for more detailed comparison of **G1** and **G2**. As we mentioned above, a photon echo experiment has showed the presence of inhomogeneous broadening in dendrimers as represented by a nonzero residual value of the peak shift (Figure 12). Static inhomogeneous broadening in the tolane-based trimer was observed in our previous experiments as well and was attributed to twisted conformers.[41] The inhomogeneous broadening might have negative impact on both the coherent domain size (by localizing excitation)[98] and the maximum TPA absorption at a particular concentration and wavelength (through "dilution effect").[71] Previously, we reported that this kind of inhomogeneity in a triple bond-based system can be completely suppressed in architectures which block twisting around the triple bond.[100] This can point to a direction for future structure optimization.

Finally, the above-mentioned photon echo experiments have provided unique information about absorption transition dipole scaling, reorganization energies, the extent of inhomogeneous broadening, and motional narrowing associated with extended spectroscopic units in large dendrimers. This information is difficult or even impossible to obtain by other spectroscopic methods. In combination with other complementary spectroscopic techniques it allows us to build a consistent spectroscopic picture of these large complex macromolecules and to correlate it with TPA properties.

4. Conclusions

In order to fully utilize the potential of macromolecular multichtomophoric systems in nonlinear optics, light harvesting, and for the efficient excitation transport for long distances we should go beyond the weak interaction limit to highly delocalized excitations where many chromophores within the system are coherently coupled. The problem of excitation delocalization length was intensively studied for linear polymers,[35−38,65,85,86] natural photosynthetic antennas,[66,75,76] and *J* aggregates.[90,91,97,98] Dendrimers are more ordered systems than linear polymers, and due to specific structure they can accommodate more chromophores in a small volume. This makes strongly interacting dendrimers with a large number of coherently coupled conjugated linear blocks very promising for nonlinear optical, excitation transport, and harvesting applications. There is no single experimental method to detect the coherent domain size. This problem intrinsically requires a multitechnique approach. The number of coherently coupled repeat units is now more or less established in most important linear polymer systems although many details remain to be clarified. This parameter is unknown for most of the large (larger than trimer) branched conjugated systems. Our paper describes the synthesis of large, strongly coupled dendrimer systems and characterizes the delocalization length by several different methods of time-resolved, nonlinear, and linear steady-state spectroscopy. We brought together most of the recent synthetic and spectroscopic techniques combined with theoretical modeling to reliably prove the presence of the excitations delocalized over nine branches in a large new dendrimer at room temperature.

It is worth emphasizing the very different spectroscopic properties (static and dynamic) of this dendrimer system as compared to those of the widely investigated phenylacetylene dendrimer family based on the same tolane connector.[29−31] The specific structure of electronic interactions associated with meta-substitutions on a phenyl ring results in fairly different spectroscopic units in the ground- and excited-state configurations with excitations localized on a single tolane segment in the ground-state geometry[29−31](which is relevant for instantaneous TPA). Comparison with our results shows (in line with

previous investigations[1−6,32−34,41,47,48,101]) that the nitrogen branching center is very beneficial for the extended delocalization and enhanced TPA.

Our detailed spectroscopic study reveals that in the new dendrimers the spectroscopic unit (domain), of fundamental importance for energy transfer and optical nonlinearities, is comparable with the size of the dendrimer **G1** and extends beyond the trimer system **G0**. The extension of the coherence domain correlates with enhanced TPA cross sections. Comparison with other branched or dendritic systems (with different charge-symmetry, or branching centers) indicates that this effect is strongly dependent on the nature of the building blocks (topology is also expected to play a role), opening a "supramodular" approach to dendritic structures with extended coherence domains.

Acknowledgment. Support of this research by National Science Foundation (DMR-Polymers, TG) and the Army Research Office (T.G.) is gratefully acknowledged. M.B.D. acknowledges financial support from DGA (Grant No. 00.34.070.00.470.75.653) and Rennes Métropole.

References and Notes

(1) Goodson, T., III. *Ann. Rev. Phys. Chem.* **2005**, *56*, 581−603.
(2) Goodson, T., III. *Acc. Chem. Res.* **2005**, *38*, 99−107.
(3) Chung, S.-J.; Kim, K.-S.; Lin, T.-C.; He, G.-S.; Swiatkiewicz, J.; Prasad, P. N. *J. Phys. Chem. B* **1999**, *103*, 10741−10745.
(4) Beljonne, D.; Wenseleers, W.; Zojer, E.; Shuuai, Z.; Vogel, H.; Pond, S. J. K.; Perry, J. W.; Marder, S. R.; Bredas, J.-L. *Adv. Funct. Mater.* **2002**, *12*, 631−641.
(5) Lahankar, S. A.; West, R.; Varnavski, O.; Xie, X.; Sukhomlinova, L.; Twieg, R.; Goodson, T., III. *J. Chem. Phys.* **2004**, *120*, 337−344.
(6) Katan, C.; Terenziani, F.; Mongin, O.; Werts, H. V.; Porres, L.; Pons, T.; Mentz, J.; Tretiak, S.; Blanchard-Desce, M *J. Phys. Chem. A.* **2005**, *109*, 3024−3037.
(7) Bar-Haim, A; Klafter, J.; Kopelman, R. *J. Am. Chem. Soc.* **1997,** *119*, 6197−6198.
(8) Jiang, D-L.; Aida, T. *Nature* **1997**, *388*, 454−456.
(9) Hagfeldt, A.; Grätzel, M. *Acc. Chem. Res.* **2000**, *33*, 269−277.
(10) Andronov, A.; Fréchet, J. M. J. *Chem. Commun.* **2000**, 1701−1710.
(11) Lo, S.-C.; Richards, G. J.; Markham, P. J.; Namdas, E. B.; Sharma, S.; Burn, P. L.; Samuel, I. D. W. *Adv. Funct. Mater.* **2005**, *15*, 1451−1458.
(12) Freeman, A. W.; Koene, S. C.; Malenfant, P. R. L.; Thompson, M. E.; Fréchet, J. M. J. *J. Am. Chem. Soc.* **2000**, *122*, 12385−12386.
(13) Fréchet, J. M. J.; Tomalia, D. *Dendrimers and Other Dendritic Polymers*; Wiley: Chichester, 2001.
(14) Newkome, G. R.; Moorefield, C. N.; Vögtle, F. *Dendritic Molecules: Concepts, Synthesis, Perspectives*; Wiley-VCH: Weinheim, Germany, 2001.
(15) Moore, J. S. *Acc. Chem. Res.* **1997**, *30*, 402−413.
(16) Deb, S. K.; Maddux, T. M.; Yu, L. *J. Am. Chem. Soc.* **1997**, *119*, 9079−9080.
(17) Pillow, J. N. G.; Halim, M. Lupton, J. M.; Burn, P. L.; Samuel, I. D. W. *Macromolecules* **1999**, *32*, 5985−5993.
(18) Lehmann, M.; Schartee, B.; Hennecke, M.; Meier, H *Tetrahedron* **1999**, *55*, 13377−13394.
(19) Adronov, A.; Gilat, S. L.; Fréchet, J. M. J.; Ohta, K.; Neuwahl, F. V. R.; Fleming, G. R. *J. Am. Chem. Soc.* **2000**, *122*, 1175−1185.
(20) Maus, M.; Mitra, S.; Lor, M.; Hofkens, J.; Weil, T.; Herrmann, A.; Müllen, K.; De Schryver, F. C. *J. Phys. Chem. A* **2001**, *105*, 3961−3966.
(21) Neuwahl, F. V. R.; Pighini, R.; Adronov, A.; Malenfant, P. R. L.; Fréchet, J. M. J. *J. Phys. Chem. B* **2001**, *105*, 1307−1312.
(22) Jiang, D-L.; Aida, T. *J. Am. Chem. Soc.* **1998**, *120*, 10895−10901.
(23) Scholes, C. D.; Jordanides, X. J.; Fleming, G. R. *J. Phys. Chem. B* **2001**, *105*, 1640−1651.
(24) Kopelman, R.; Shortreed, M.; Shi, Z.-Y.; Tan, W.; Xu, Z.; Moore, J. S.; Bar-Haim, A.; Klafter, J. *Phys. Rev. Lett.* **1997**, *78*, 1239−1242.
(25) Tretiak, S.; Chernyak, V.; Mukamel, S. *J. Phys. Chem. B* **1998**, *102*, 3310−3315.
(26) Heijs, D-J.; Malyshev, V. A.; Knoester, J. *J. Chem. Phys.* **2004**, *121*, 4884−4892.
(27) Varnavski, O.; Samuel, I. D. W.; Pålsson, L.-O.; Beavington, R.; Burn, P. L.; Goodson, T., III. *J. Chem. Phys.* **2002**, *116*, 8893−8903.
(28) Drobizhev, M.; Karotki, A.; Dzenis, Y.; Rebane, A.; Suo, Z.; Spangler, C. W. *J. Phys. Chem. B* **2003**, *107*, 7540−7543.
(29) Devadoss, C.; Bharathi, P.; Moore, J. S. *J. Am. Chem. Soc.* **1996,** *118*, 9635−9644.
(30) Devadoss, C.; Bharathi, P.; Moore, J. S. *Macromolecules* **1998,** *31*, 8091−8099.
(31) Thompson, A. L.; Gaab, K. M.; Xu, J.; Bardeen, C. J.; Martinez, T. J. *J. Phys. Chem. A* **2004**, *108*, 671−682.
(32) Drobizhev, M.; Rebane, A.; Suo, Z.; Spangler, C. W. *J. Lumin.* **2005**, *111*, 291−305.
(33) Wang, Y.; He, G. S.; Prasad, P. N.; Goodson, T., III. *J. Am. Chem. Soc.* **2005**, *127*, 10128−10129.
(34) Ranasinghe, M. I.; Varnavski, O. P.; Pawlas, J.; Hausk, S. I.; Louie, J.; Hartwig, J. F.; Goodson, T., III. *J. Am. Chem. Soc.* **2002**, *124*, 6520−6521.
(35) Grage, M. M.-L.; Zaushitsyn, Y.; Yartsev, A.; Chachisvilis, M.; Sundström, V.; Pullerits, T. *Phys. Rev. B* **2003**, *67*, 205207.
(36) Beenken, W. J. D.; Pullerits, T. *J. Phys. Chem. B* **2004**, *108*, 6164−6169.
(37) Yang, X.; Dykstra, T. E.; Scholes, G. D. *Phys. Rev. B* **2005**, *71*, 045203.
(38) Schindler, F.; Jacob, J.; Grimsdale, A. C.; Scherf, U.; Müllen, K.; Lupton, J. M.; Feldmann, J. *Angew. Chem., Int. Ed.* **2005**, *44*, 1520−1525.
(39) Tretiak, S.; Mukamel, S. *Chem. Rev.* **2002**, *102*, 3171−3212.
(40) Varnavski, O. P.; Ranasinghe, M.; Yan, X.; Bauer, C. A.; Chung, S.-J.; Perry, J. W.; Marder, S. R.; Goodson, T., III. *J. Am. Chem. Soc.* **2006**, *128*, 10988−10989.
(41) Varnavski, O.; Sukhomlinova, L.; Twieg, R., Goodson, T., III. *J. Phys. Chem. B* **2004**, *108*, 10484−10492.
(42) Porrès, L.; Mongin, O.; Katan, C.; Charlot, M.; Pons, T.; Mertz, J.; Blanchard-Desce, M. *Org. Lett.* **2004**, *6*, 47−50.
(43) Hawker, C. J.; Fréchet, J. M. J. *J. Am. Chem. Soc.* **1990**, *112*, 7638−7647.
(44) Käpplinger, C.; Beckert, R. *Synthesis* **2002**, 1843−1850.
(45) Mongin, O.; Porrès, L.; Moreaux, L.; Mertz, J.; Blanchard-Desce, M. *Org. Lett.* **2002**, *4*, 719−722.
(46) Xu, C.; Webb, W. W. *J. Opt. Soc. Am. B* **1996**, *13*, 481−491.
(47) Varnavski, O.; Menkir, G.; Goodson, T., III; Burn, P. L.; Samuel, I. D. W.; Lupton, J. M.; Beavington, R. *Appl. Phys. Lett.* **2000**, *77*, 1120−1122.
(48) Varnavski, O. P.; Ostrovski, J. C.; Sukhomlinova, L.; Twieg, R. J.; Bazan, G. C.; Goodson, T., III. *J. Am. Chem. Soc.* **2002**, *124*, 1736−1743.
(49) Mukamel, S. *Principles of Nonlinear Optical Spectroscopy*; Oxford: New York, 1995.
(50) Cho, M. H.; Yu, J. Y.; Yoo, T.; Nagasawa, Y.; Passino, S. A.; Fleming, G. R. *J. Phys. Chem.* **1996**, *100*, 11944−11953.
(51) de Boeij, W. P.; Pshenichnikov, M. S.; Wiersma, D. A. *J. Phys. Chem.* **1996**, *100*, 11806−1823.
(52) Joo, T.; Jia, Y.; Yu, J.-Y.; Lang, M. J.; Fleming, G. R. *J. Chem. Phys.* **1996**, *104*, 6089−6108.
(53) Galagher Faeder, S. M.; Jonas, D. M. *Phys. Rev. A* **2000**, *62*, 033820.
(54) Nagasawa, Y.; Passino, S. A.; Yoo, T.; Fleming, G. R. *J. Chem. Phys.***1997**, *106*, 4840−4851.
(55) Hirata, Y.;Okada, T.; Nomoto, T.; Mataga, N. *J. Phys. Chem.* **1996**, *96*, 6559−6563.
(56) Hirata, Y.; Okada, T.; Nomoto, T. *Chem. Phys. Lett.* **1998**, *293*, 371−377.
(57) Okuyama, K.; Hasegawa, T.; Ito, M.; Mikami, N. *J. Phys. Chem.* **1984**, *88*, 1711−1716.
(58) Murrel, J. N. *The Theory of Electronic Spectra of Organic Molecules*; Willey: New York, 1973.
(59) Latterini, L.; De Belder, G.; Schweitzer, G.; Van der Auweraer, M.; De Schryver, F. C. *Chem. Phys. Lett.* **1998**, *295*, 11−16.
(60) Verbouwe, W.; Van der Auweraer, M.; Piet, J. J.; Warman, J. M.; De Schryver, F. C. *J. Am. Chem. Soc.* **1998**, *120*, 1319−1324.
(61) Bangal, P. R.; Lam, D. M. K.; Peteanu, L. A.; Van der Auweraer, M. *J. Phys. Chem. B* **2004**, *108*, 16834−16840.
(62) Yeh, A. T.; Shank, C. V.; McCusker, J. K. *Science* **2000**, *289*, 935−938.
(63) van Velhoven, E.; Zhang, H.; Glasbeek, M. *J. Phys. Chem. A* **2001**, *105*, 1687−1692.
(64) Shaw, G. B.; Brown, C. L.; Papanikolas, J. M. *J. Phys. Chem. A* **2002**, *106*, 1483−1495.
(65) Tretiak, S.; Saxena, A.; Martin, R. L.; Bishop, A. R. *Phys. Rev. Lett.* **2002**, *89*, 097402.
(66) Leopold, D.; Stiel, H.; Teuchner, K.; Nowak, F.; Sandner, W.; Ücker, B.; Scheer, H. *Phys. Rev. Lett.* **1996**, *77*, 4675−4678.
(67) Adronov, A.; Fréchet, J. M. J.; He, G. S.; Kim, K.-S.; Chung, S.-J.; Lin, Swiatkiewicz, J.; Prasad, P. N. *Chem. Mater.* **2000**, *12*, 2838−2841.
(68) Strickler, S. J.; Berg, R. A. *J. Chem. Phys.* **1962**, *37*, 814−822.
(69) Ranasinghe, M. I.; Hager, M. W.; Gorman, C. B.; Goodson, T., III. *J. Phys. Chem. B* **2004**, *108*, 8543−8549.

(70) Drobizhev, M.; Rebane, A.; Blanchard-Desce, M. Manuscript in preparation.

(71) Kuzyk, M. *J. Chem. Phys.* **2003**, *119*, 8327−8334.

(72) Porrès, L.; Katan, C.; Mongin, O.; Pons, T.; Mertz, J.; Blanchard-Desce, M. *J. Mol. Struct.* **2004**, *704*, 17−24.

(73) Soutar, I.; Swanson, L.; Christensen, R. L.; Drake, R.; Phillips, D. *Macromolecules* **1996**, *29*, 4931−4936.

(74) Cross, A. J.; Fleming, G. R. *Biophys. J.* **1984**, *46*, 45−56.

(75) Bradforth, S. E.; Jimenez, R.; van Mourik, F.; van Grondelle, R.; Fleming, G. R. *J. Phys. Chem.* **1995**, *99*, 16179−16191.

(76) Leegwater, J. A. *J. Phys. Chem.* **1996**, *100*, 14403−14409.

(77) Horng, M. L.; Gardecki, J. A.; Papazyan, A.; Maroncelli, M. *J. Phys. Chem.* **1995**, *99*, 17311−17337.

(78) Wavelength-resolved femtosecond transient absorption results as well as exciton−exciton annihilation experiments in these dendrimers will be published elsewhere: Ramakrishna, G; Yan, X.; Varnavski, O.; Mongin, O.; Blanchard-Desce, M.; Goodson, T., III. Manuscript in preparation.

(79) Knox, R.; Gulen, D. *Photochem. Photobiol.* **1993**, *57*, 40−43.

(80) Wynne, K.; Hochstrasser, R. M. *Chem. Phys.* **1993**, *171*, 179−188.

(81) Agarwal, R.; Rizvi, A. H.; Prall, B. S.; Olsen, J. D.; Hunter, C. N.; Fleming, G. R. *J. Phys. Chem. A* **2002**, *106*, 7573−7578.

(82) Salvador, M. R.; Hines, M. A.; Scholes, G. D. *J. Chem. Phys.* **2003**, *118*, 9380−9388.

(83) Meier, T.; Chernyak, V.; Mukamel, S. *J. Chem. Phys.* **1997**, *107*, 8759−8780. Along with the transition dipole moment, the dephasing-related factor can be presented in the photon echo intensity scaling law: integrated echo intensity reads

$$S_{PE}(\tau) \approx \int |P^{(3)}|^2 \mathrm{d}t$$

with:

$$P^{(3)}(\tau,T,t) \propto \int \mathrm{d}t'_3 \int \mathrm{d}t'_2 \int \mathrm{d}t'_1 \sum_{i=1}^{4} R_i(t'_1,t'_2,t'_3) \times \vec{E}_1^*(\vec{k}_1,t_1)\vec{E}_2(\vec{k}_2,t_2)\vec{E}(\vec{k}_3,t_3)$$

$P^{(3)}$ third-order nonlinear polarization, $R_i(t_1, t_2, t_3)$ nonlinear response functions, electric fields E_i. For Bloch limit and two-level system:

$$P^{(3)} \propto \mu_{\mathrm{eg}}^4 \exp\left[-\left(\frac{t-\tau}{2T_2^*}\right)^2\right] \exp\left[-\frac{t+\tau}{T_2}\right],$$

which results in

$$S_{PE\mathrm{int}} \propto \frac{\mu_{\mathrm{eg}}^8}{\Delta\omega_{\mathrm{inh}}} \exp\left(-\frac{4\tau}{T_2}\right)$$

for integrated echo or in the limit of a long excitation pulse:

$$S_{PE\mathrm{int}} \propto \mu_{\mathrm{eg}}^8 T_2^* T_2$$

($\Delta\omega_{\mathrm{inh}}=1/T_2^*$ = inhomogeneous linewidth; T_2 = "pure" (homogeneous) dephasing time). In our case the linewidths are comparable for all dendrimer generations, and the transition dipole moment to the eighth power should dominate the scaling.

(84) Ledox, I.; Samuel, I. D. W.; Zyss, J.; Yaliraki, S. N.; Schattermann, F. J.; Schrock, R. R.; Silbey, R. J. *Chem. Phys.* **1999**, *245*, 1−16.

(85) Samuel, I. D. W.; Ledox, I.; Dhenaut, C.; Zyss, J.; Fox, H. H.; Schrock, R. R.; Silbey, R. J. *Science* **1994**, *265*, 1070−1072.

(86) Jimenez, R.; van Mourik, F.; Yu, J. Y.; Fleming, G. R. *J. Phys. Chem. B* **1997**, *101*, 7350−1759.

(87) Salverda, J. M.; van Mourik, F.; van der Zwan, G.; van Grondelle, R. *J. Phys. Chem. B* **2000**, *104*, 11395−11408.

(88) Yang, M.; Agarwal, R.; Fleming, G. R. *J. Photochem. Photobiol.* **2001**, *142*, 107−119.

(89) Yu, J.-Y.; Nagasawa, Y.; van Grondelle R.; Fleming, G. R. *Chem. Phys. Lett.* **1997,** *280*, 404−410.

(90) Lee, J.-H.; Min, C.-K.; Joo, T. *J. Chem. Phys.* **2001**, *114*, 377−381.

(91) Ohta, K.; Yang, M.; Fleming, G. R. *J. Chem. Phys.* **2001**, *115*, 7609−7621.

(92) Jimenez, R.; Salazar, G.; Baldridge, K. K.; Romesberg, F. E. *Proc. Natl. Acad. Sci. U.S.A.* **2003**, *100*, 92−97.

(93) Jimenez, R.; Case, D. A.; Romesberg, F. E. *J. Phys. Chem. B* **2002**, *106*, 1090−1103.

(94) Larsen, D. S.; Ohta, K.; Xu, Q.-H.; Cyrier, M.; Fleming, G. R. *J. Chem. Phys.* **2001**, *114*, 8008−8019.

(95) Ohta, K.; Larsen, D. S.; Yang, M.; Fleming, G. R. *J. Chem. Phys.* **2001**, *114*, 8020−8039.

(96) Larsen, D. S.; Ohta, K.; Fleming, G. R. *J. Chem. Phys.* **1999**, *111*, 8970−8979.

(97) Knapp, E. W. *Chem. Phys.* **1984**, *85*, 73−82.

(98) Fidder, H.; Knoester, J.; Wiersma, D. A. *J. Chem. Phys.* **1991**, *95*, 7880−7890.

(99) Yang, J.-S.; Chiou, S.-Y.; Lian, K.-L. *J. Am. Chem. Soc.* **2002**, *124*, 2518−2527.

(100) Anand, S.; Varnavski, O.; Marsden, J. A.; Haley, M. M.; Schlegel, H. B.; Goodson, T., III. *J. Phys. Chem. A* **2006**, *110*, 1305−1318.

(101) Wang, Y.; Ranasinghe, M.; Goodson, T., III. *J. Am. Chem. Soc.* **2003**, *125*, 9562−9563.